Cell & Bioscience

RESEARCH

Open Access

Modelling porcine NAFLD by deletion of leptin and defining the role of AMPK in hepatic fibrosis

Tan Tan[1,2†], Zhiyuan Song[1†], Wenya Li[1], Runming Wang[1], Mingli Zhu[1], Zuoxiang Liang[1], Yilina Bai[1], Qi Wang[1], Hanyu Wu[1], Xiaoxiang Hu[1] and Yiming Xing[1*]

Abstract

Background Non-alcoholic fatty liver disease (NAFLD) is the most prevalent cause of chronic hepatic disease and results in non-alcoholic steatohepatitis (NASH), which progresses to fibrosis and cirrhosis. Although the Leptin deficient rodent models are widely used in study of metabolic syndrome and obesity, they fail to develop liver injuries as in patients.

Methods Due to the high similarity with humans, we generated Leptin-deficient (*Leptin*$^{-/-}$) pigs to investigate the mechanisms and clinical trials of obesity and NAFLD caused by Leptin.

Results The *Leptin*$^{-/-}$ pigs showed increased body fat and significant insulin resistance at the age of 12 months. Moreover, *Leptin*$^{-/-}$ pig developed fatty liver, non-alcoholic steatohepatitis and hepatic fibrosis with age. Absence of Leptin in pig reduced the phosphorylation of JAK2-STAT3 and AMPK. The inactivation of JAK2-STAT3 and AMPK enhanced fatty acid β-oxidation and leaded to mitochondrial autophagy respectively, and both contributed to increased oxidative stress in liver cells. In contrast with *Leptin*$^{-/-}$ pig, although Leptin deletion in rat liver inhibited JAK2-STAT3 phosphorylation, the activation of AMPK pathway might prevent liver injury. Therefore, β-oxidation, mitochondrial autophagy and hepatic fibrosis did not occurred in *Leptin*$^{-/-}$ rat livers.

Conclusions The Leptin-deficient pigs presents an ideal model to illustrate the full spectrum of human NAFLD. The activity of AMPK signaling pathway suggests a potential target to develop new strategy for the diagnosis and treatment of NAFLD.

Keywords Liver fibrosis, LEPTIN, Pig, NAFLD, AMPK pathway

Background

Liver fibrosis is a common result of chronic damage to the liver caused by the accumulation of extracellular matrix proteins. A number of liver diseases as well as side effects of some drugs lead to liver fibrosis. Among these causes, non-alcoholic steatohepatitis (NASH) has been recognized as a major etiology [1]. It is considered part of the spectrum of non-alcoholic fatty liver disease (NAFLD) [2]. Excessive adipose tissue in NAFLD patients leads to an inflammatory state targeting liver parenchyma with steatosis and fibrosis observed in a

†Tan Tan and Zhiyuan Song authors contributed equally to this work.

*Correspondence:
Yiming Xing
ymxing@cau.edu.cn
[1] State Key Laboratory of Animal Biotech Breeding, College of Biological Science, China Agricultural University, Beijing, People's Republic of China
[2] Development Center of Science and Technology, Ministry of Agriculture and Rural Affairs, Beijing, People's Republic of China

significant portion of cases. Hepatic fibrogenesis can progress to cirrhosis which enhances the risk of hepatocellular carcinoma. Alarmingly, few effective pharmacotherapeutic approaches are currently available to block or attenuate development and progression of NAFLD. Liver transplantation is the only efficient treatment option in patients with decompensated cirrhosis [3]. Nowadays, the fibrosis stage is viewed as the most important predictor of mortality in NAFLD. However, it is not a unidirectional progressive process, ultimately leading to liver cirrhosis and organ failure, but is in principle reversible. Accordingly, better understanding of mechanisms underlying fibrogenesis are crucial for the development of new strategies for the prevention and treatment of NAFLD and other related liver disease.

Although the pathogenesis of liver fibrosis has not been fully discovered, the primary role is played by the deposition of triglycerides in liver cells and the formation of lipid droplets [4]. An accumulation of fatty liver leads to insulin resistance in adipose tissue with increased proinflammatory cytokines, which initiate the necrosis and apoptosis of liver cells [5]. Elevated free fatty acid (FFA) aggravates the oxidative damage of liver cells, and also leads to insulin resistance. Insulin resistance worsens adipocyte function and promotes the transition of NASH to overt liver fibrosis [6]. Although the mechanism of fibrosis deposition has been identified, there are almost no therapies currently available that directly prevent or reverse it. While animal models have been indispensable in further studies, current models possess important limitations which largely restricted the understanding of the underlying mechanism driving fibrosis development and discovery of new diagnostics and therapeutics for NAFLD and other liver disease.

Leptin and its receptor play an important role in driving the formation of liver fibrosis. Leptin is an adipocyte-derived hormone that mediates energy homeostasis in various ways, including regulating energy metabolism, promoting oxidation of FFAs and inhibiting fat synthesis [7]. A substantial subset of obese patients have relatively low circulating levels of Leptin. Leptin-deficient (*ob/ob*) mice and Leptin receptor-deficient (Zucker) rats are widely used for studying the mechanisms underlying the role of Leptin in hepatic fibrosis. However, these models only represent fatty liver, but not fibrosis in the spontaneous state. Although compounds such as thioacetamide or carbon tetrachloromethane have been shown to behave as potent hepatotoxins which trigger hepatic injury and lead to development of fibrosis, these models cannot fully reflect the unembellished transformation of steatohepatitis to fibrosis in NAFLD patients, either in disease spectrum or etiology [8, 9].

This study aimed to investigate the mechanisms of liver fibrosis and NAFLD caused by Leptin deficiency. Due to the high similarity in physiology and metabolism between humans and pigs, we generated the *LEPTIN*$^{-/-}$ pig, which simulates the progression of liver injury, from fatty liver to NASH and hepatic fibrosis, the general physiological alterations and the pathological patterns of NAFLD patients. Compared with *Leptin*$^{-/-}$ rats, we discovered that the alteration of JAK2-STAT3 and AMPK signaling pathways mediates β-oxidation and mitochondrial autophagy respectively in *LEPTIN*$^{-/-}$ pigs, which in turn enhanced oxidative stress and promoted the development of fatty liver to fibrosis. The *LEPTIN*$^{-/-}$ pig model provides a valuable tool to discover the mechanism of the progression of hepatic fibrosis. Meanwhile, the activity of AMPK signaling pathway suggests a potential target to develop new strategy for the diagnosis and treatment of NAFLD.

Results

LEPTIN deletion in pigs causes obesity

To generate LEPTIN-knockout pigs, exon 2 of the porcine *LEPTIN* gene was targeted using ZFNs vectors (Fig. 1, Additional file 1: Fig. S1A, B). The mutant pig fetal fibroblasts cell clones were screened and transplanted using somatic cell nuclear transfer to generate transgenic pigs. Through DNA sequencing, various mutants were identified in the transgenic pigs (Fig. 1, Additional file 1: Fig. S1C, D). As a matter of convenience, mutants were grouped as *LEPTIN*$^{-/-}$ and *LEPTIN*$^{\pm}$. The expression of *LEPTIN* were nearly undetectable in *LEPTIN*$^{-/-}$ subcutaneous and visceral fat (Fig. 1, Additional file 1: Fig. S2A). The LEPTIN protein was not detected in *LEPTIN*$^{-/-}$ serum (Fig. 1, Additional file 1: Fig. S2B). In order to determine whether the ZFNs resulted in off-target mutations, the genomic regions with the highest levels of homology were analyzed. No off-target mutations were observed at any of the sites profiled using PCR amplification and sequencing (Additional file 1: Table S1).

Multiple studies have observed that Leptin plays an important role in the development of obesity. Both wild type and *LEPTIN*$^{-/-}$ pigs were provided with same manufactured diet. Formula feed is premixed based on the animal's nutritional requirements to meet different stages of growth. The nutrition content per kg premix formula feed is listed in Table 1. The *LEPTIN*$^{-/-}$ pigs obtained nearly twice the body weight vs control pigs at 21-months of age (103.75 ± 12.37 kg vs 56.50 ± 8.49 kg) (Fig. 1A, B). By MSCT, both subcutaneous and abdominal visceral fat were significantly increased in *LEPTIN*$^{-/-}$ compared to control pigs (Fig. 1C), and the maximum thickness of subcutaneous fat and the percentage of body fat were more than three times that of control pigs (Fig. 1,

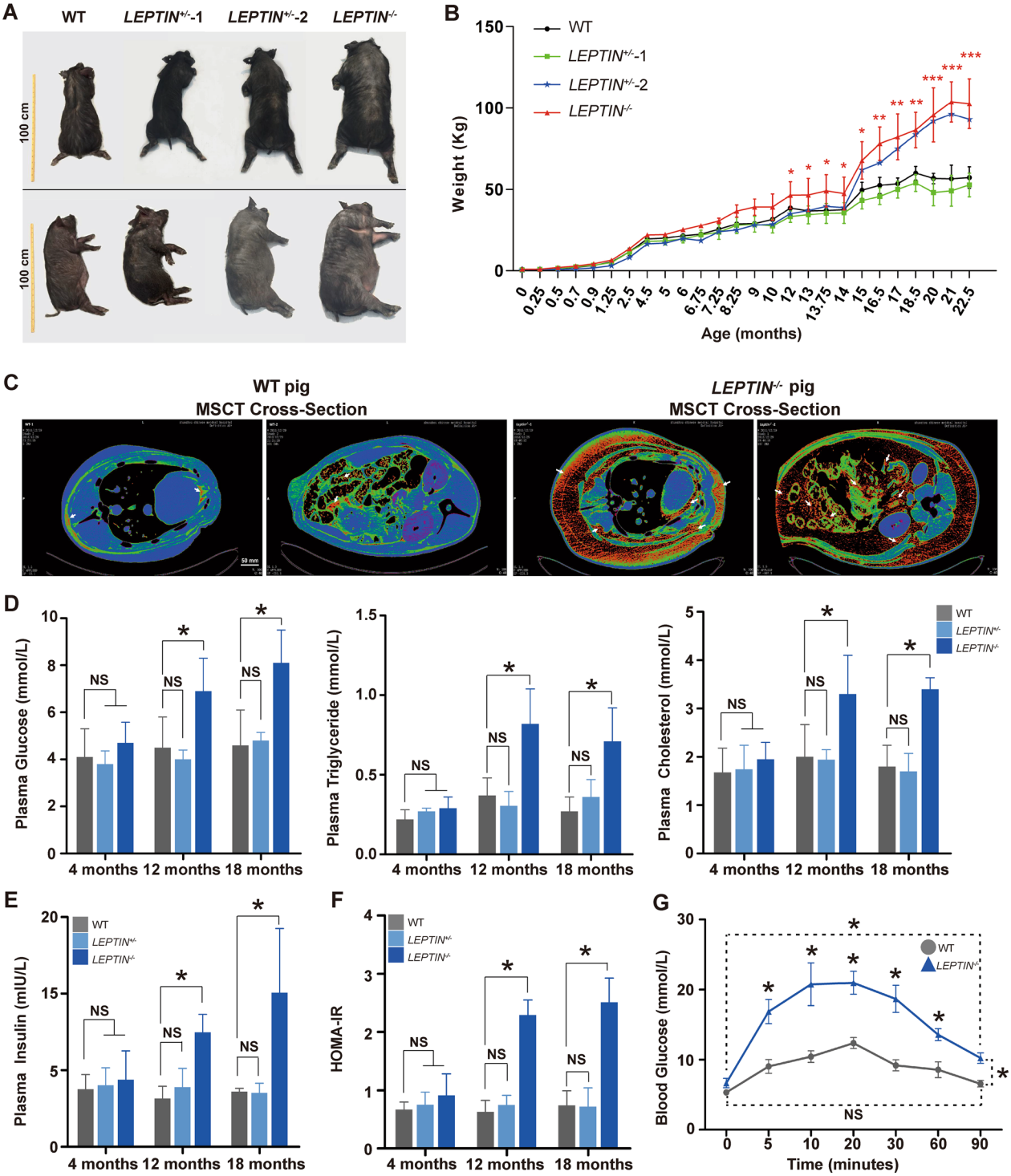

Fig. 1 Generation and phenotyping of *LEPTIN*$^{-/-}$ pigs. **A** Body sizes of *LEPTIN* mutant and WT pigs. Yellow scale bar represents 1 m. **B** Monthly weight records of pigs. N = 3/group. **C** MSCT scan tomography showing body fat distribution in *LEPTIN* mutant and WT pigs. The red area and white arrows indicated adipose tissue. The scale bar represents 50 mm. **D** Blood glucose, plasma triglyceride and plasma total cholesterol levels in *LEPTIN* mutant and WT pigs. **E** Plasma insulin levels in *LEPTIN* mutant and WT pigs. **F** HOMA-IR results evaluating insulin resistance for pigs at different ages. **G** IVGTT assay to assess blood glucose regulation. N = 3/group. The bars represent the mean ± SD; *P < 0.05, **P < 0.01, and ***P < 0.001; NS, non-significant

Table 1 Composition and nutrient levels of diets used in this study

Growth stage	Feed	Feed stuff	Guaranteed value of component analysis	Feed additives
Nutrition content of pig diets				
Weaning-45 Days	*AnYou-810* formula feed for suckling pigs (Anyou Feed Co. LTD, China)	Bean pulp, corn particle, Flour. soybean oil, sodium chloride, choline chloride, copper sulfate, zinc chloride, manganese sulfate, L -lysine hydrochloride, DL-methionine, Vitamin A, E, D3, phytase	Crude protein (%) ≥ 19.5, crude fat (%) ≥ 2.8, crude ash (%) ≤ 8.0, crude fiber ≤ 4.0, calcium (%) 0.5–1.1, total phosphorus (%) ≥ 0.3, sodium chloride (%) 0.3–0.9. lysine (%) ≥ 1.6. water (%) ≤ 14.0	Aureomycin premix 75 mg/kg, Kitasamycin premix 50 mg/kg, Bacitritin zinc premix 40 mg/kg
45–85 Days	*MuWang-352* formula feed for piglets (MuWang Feed Co. LTD China)	Corn, soybean meal, soybean oil, calcium hydrogen phosphate, calcium carbonate, sodium chloride, lysine, vitamin A, D3, E, K3, B12, copper sulfate, zinc sulfate. manganese sulfate, ferrous sulfate, sodium selenite, calcium iodate	Crude protein (%) ≥ 17.5, crude ash (%) ≤ 7.0, crude fiber ≤ 5.0, calcium (%) 0.5–1.0. total phosphorus (%) ≥ 0.5. sodium chloride (%) 0.3–0.8, lysine (%) ≥ 1.0, water (%) ≤ 14.0	Aureomycin premix 72 mg/kg, Flavamycin premix 24 mg/kg
85 Days	*Purina-832980* formula feed for boar (Agribrands Purina Feedmill (Langfang) Co., Ltd, USA & China)	Corn, soybean meal, bran, calcium hydrogen phosphate, calcium carbonate, sodium chloride, L-lysine, vitamins A, D3, E, B2, B12, copper sulfate, ferrous sulfate, zinc sulfate, manganese sulfate, sodium nitrite, phytase, etc	Crude protein (%) ≥ 13, crude ash (%) ≤ 10.0, crude fiber ≤ 10.0, calcium (%) 0.4–1.5, total phosphorus (%) ≥ 0.3. sodium chloride (%) 0.3–0.1.5, lysine (%) ≥ 0.45, water (%) ≤ 14.0	–
Sow pregnancy	*MuWang-356* formula feed for piglets (MuWang Feed Co. LTD, China)	Corn, soybean meal, soybean oil, calcium hydrogen phosphate, calcium carbonate, sodium chloride, lysine, vitamin A, D3, E, K3, B12, copper sulfate, zinc sulfate, manganese sulfate, ferrous sulfate, sodium selenite, calcium iodate	Crude protein (%) ≥ 14.0. crude ash (%) ≤ 8.0, crude fiber ≤ 7.0, calcium (%) 0.6–0.95, total phosphorus (%) ≥ 0.5. sodium chloride (%) 0.3–0.8, lysine (%) 0.65, water (%) ≤ 14.0	–
Lactation period	*MuWang-357* formula feed for piglets (MuWang Feed Co. LTD, China)	Corn, soybean meal, soybean oil. calcium hydrogen phosphate. calcium carbonate, sodium chloride, lysine, vitamin A, D3, E, K3, B12, copper sulfate, zinc sulfate manganese sulfate, ferrous sulfate, sodium selenite, calcium Iodate	Crude protein (%) ≥ 16.0. crude ash (%) ≤ 8.0. crude fiber ≤ 7.0. calcium (%) 0.6–0.95, total phosphorus (%) ≥ 0.5, sodium chloride (%) 0.3–0.8, lysine (%) 0.8, water (%) ≤ 14.0	–
Nutrition content of rat diets				
Weaning-growth	*HuaFukang*-1022 Rat growth maintenance feed (Beijing Hua Fu Kang Biotechnology Co. LTD, China)		Soybean meal, fish meal, Vegetable oil, bran, corn, Vitamins A, D, E, B1, B12, B6, Pantothenic acid, calcium bicarbonate, Calcium carbonate, copper sulfate, zinc sulfate, manganese sulfate, ferrous sulfate	Crude protein (%) ≥ 18.0, crude fat (%) ≥ 4.0, crude ash (%) ≤ 8.0, crude fiber ≤ 5.0, calcium (%) 1.0–1.8, total phosphorus (%) 0.6–1.2, water (%) ≤ 10.0

In this table, the composition and nutrient levels of each diets used in the study for pig and rat are listed in details

Additional file 1: Fig. S3A). Using H&E staining *LEPTIN*$^{-/-}$ adipocytes also showed increased volumes (Fig. 1, Additional file 1: Fig. S3B).

In order to determine whether LEPTIN deficiency altered clinical indicators of liver disease as observed in obese patients, blood was collected from pigs at 4-, 12- and 18-months of age. Compared to control pigs, the concentration of glucose, triglycerides, total cholesterol and low density lipoprotein (LDL) were significantly increased, while high density lipoprotein (HDL) was reduced in *LEPTIN*$^{-/-}$ serum at the 12-month and 18-month time points (Fig. 1D, Additional file 1: Fig. S4). The tendency of these blood tests is similar to that of obese patients which indicate that *LEPTIN*$^{-/-}$ pigs demonstrate clinical signs of obesity by 12-months of age.

LEPTIN deletion in pigs causes type II diabetes

Obesity is one of the main factors contributing to type II diabetes in humans. Consistent with the observed increase in obesity, insulin levels in *LEPTIN*$^{-/-}$ pigs were significantly increased at 12- and 18-months of age (Fig. 1E). By applying HOMAs to identify diabetic pigs, the insulin and blood glucose parameters indicated that the *LEPTIN*$^{-/-}$ pigs were insulin resistance by 12-months of age, with reduced insulin sensitivity and islet β cell function (Fig. 1F, Additional file 1: Fig. S5A). Histological analysis demonstrated that the size of *LEPTIN*$^{-/-}$ islets and the number of islet β cell were also increased (Fig. 1, Additional file 1: Fig. S5B).

Abnormal glucose metabolism is an essential feature of type II diabetes mellitus patients. Thus IVGTT was conducted to determine the pig's ability to regulate blood glucose. Following the injection of highly concentrated glucose, the glucose concentration in *LEPTIN*$^{-/-}$ pigs instantaneously increased to almost 20 mmol/L in 10 min, which was significantly higher than WT pigs. By 90 min post injection, the blood glucose concentration in *LEPTIN*$^{-/-}$ pigs was still higher than initial levels (10 mmol/L), whereas the WT pigs were nearly fully recovered (Fig. 1G). Thus, the lack of LEPTIN negatively affects insulin mediated glucose metabolism, further obstructing glucose regulation and contributing to type II diabetes.

LEPTIN deletion in pigs results in NAFLD

The incidence rate of non-alcoholic liver injury in obese patients is as high as 90% [12]. By the age of 0–6 months, the H&E staining and oil red O staining results showed no visible morphological differences between *LEPTIN*$^{-/-}$ and WT livers (normal/total individuals = 3/3, 100%) (Fig. 2A). However, by the age of 6–12 months, the lipid deposition and hepatocyte steatosis in *LEPTIN*$^{-/-}$ pig livers increased (injured/total individuals = 3/5, 60%) (Fig. 2B). In addition, the triglycerides and the expression of FFA synthesis related genes (*FABP1*, *FASN*, *ELOVL6*, *SCD1* and *PPARA*) were increased significantly in *LEPTIN*$^{-/-}$ pigs (Fig. 3A, B). H&E and PAS staining of *LEPTIN*$^{-/-}$ pig livers at 12–22 months of age revealed features of early stage fatty liver disease; whereas the hepatocytes demonstrated obvious balloon degeneration and vacuolated necrosis consistent with middle and late stages. In addition, a large number of mononuclear cells infiltrated the hepatic lobule portal area and between the hepatic parenchymal cells of hepatic lobules. The PAS assay showed carbohydrate components accumulated in *LEPTIN*$^{-/-}$ pig livers (Fig. 2C). Real-time PCR results confirmed the expression of *TNFA*, *IL6*, *NFKB*, *IL1B* and *MCP1*, a series of cytokines, were significantly up-regulated in the *LEPTIN*$^{-/-}$ pig liver (Fig. 3C). IL-1β, TNF-α and IL6 serum concentrations were also significantly increased (damaged individuals/total individuals = 2/6, 33%) (Fig. 3D).

Liver fibrosis, classified as the third stage of non-alcoholic liver injury, is the last step of the reversible damage process observed clinically. *LEPTIN*$^{-/-}$ pig livers obtained from animals between 22 to 35 months of age demonstrated a high degree of hepatomegaly with the presence of surface fiber bundles and granule (Fig. 2D). H&E staining demonstrated that the overall lobule structure was disorganized, and the fibrous septum of the portal area was significantly widened with distinct bridging lesions occurring in the portal and central vein areas in *LEPTIN*$^{-/-}$ pig livers (Figs. 2D and 3E). Meanwhile, Sirius Red staining revealed collagen accumulation around the hepatic lobule sinus and veins in *LEPTIN*$^{-/-}$ pig livers (damaged individuals/total individuals = 3/7, 42.9%) (Fig. 2D). Immunofluorescence staining demonstrated that the expression of α-SMA, a marker of fibrosis, was significantly up-regulated in *LEPTIN*$^{-/-}$ livers (Fig. 3E). In the clinical diagnosis of liver fibrosis, blood indexes are used to stage the disease. In this study, the fasting blood samples were collected from *LEPTIN*$^{-/-}$ and WT pigs. The results showed that ALT and AST levels in *LEPTIN*$^{-/-}$ blood were greatly increased, indicating significant liver damage. However, comparing with WT, the level of ALP remained unchanged (Fig. 3F). The levels of HA and PCIIINP in *LEPTIN*$^{-/-}$ serum were significantly elevated, indicating that fibrogenesis had occurred, although the levels of LN and CIV demonstrated no differences between *LEPTIN*$^{-/-}$ and WT livers (Fig. 3F). These suggest that the severity of the fibrotic lesions in *LEPTIN*$^{-/-}$ livers was most likely in the middle or advanced stage of fibrosis but not cirrhosis. The expression of fibrotic markers, *TGFB*, *ACTA2*, *LRAT* and *COL1A1*, were increased greatly in *LEPTIN*$^{-/-}$ livers (Fig. 3G). Previous studies had shown that *CTHRC1*

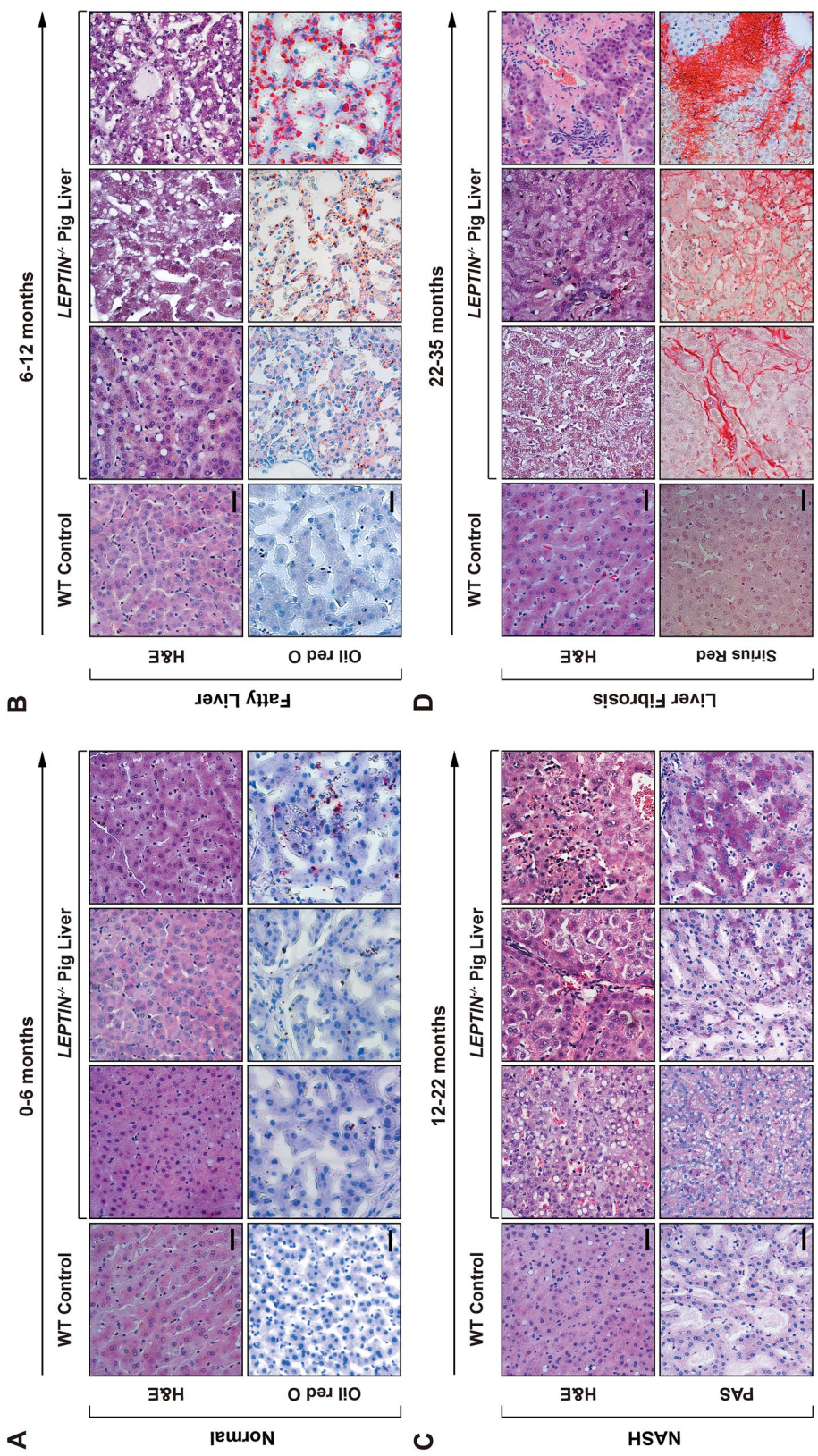

Fig. 2 Progression of liver injury in *LEPTIN*$^{-/-}$ pigs. H&E and stage-specific staining demonstrating histological alterations and injury of hepatocytes in *LEPTIN* mutant and WT pigs over time. Oil red O staining for lipid deposition (**A**, **B**), PAS staining for glycogen storage (**C**), and sirius red staining for collagen deposition (**D**). Scale bar represents 50 μm

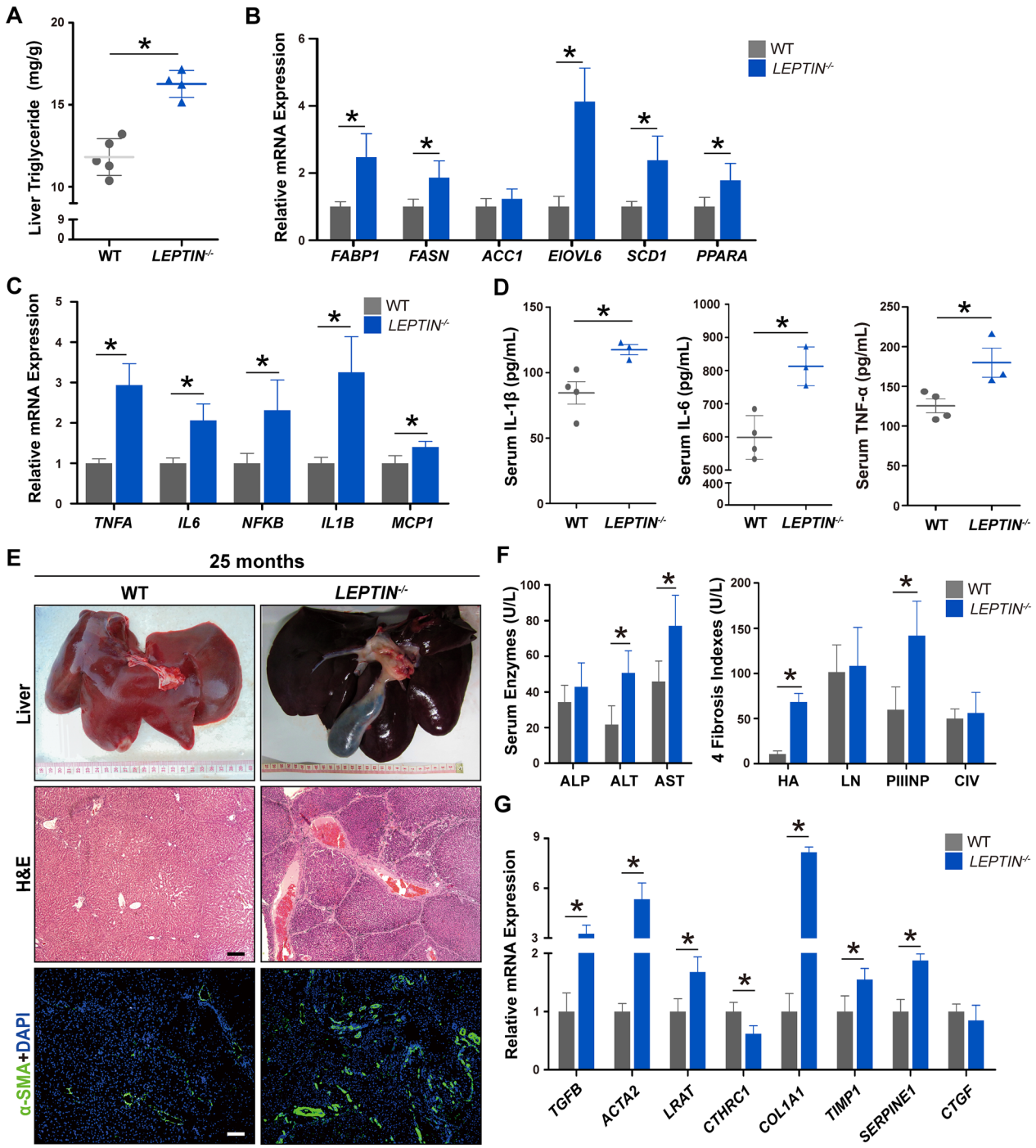

Fig. 3 Pathological and molecular detection of liver injury in *LEPTIN*$^{-/-}$ pigs. Triglyceride concentrations (**A**) and expression of genes related to FFA synthesis (**B**) in *LEPTIN* mutant and WT pigs. Expression of inflammation related genes in liver (**C**) and the concentration of inflammatory cytokines, IL-1β, IL-6 and TNF-α in serum (**D**). N = 3–5/group. **E** Gross images, H&E and immunofluorescent staining for α-SMA in 25-month-old *LEPTIN* mutant and WT livers (bar = 20 μm). **F** Liver functional status and expression of liver fibrosis markers in serum. **G** Expression of genes related to fibrogenesis. N = 3–5/group. The bars represent the mean ± SD; *P < 0.05; *NS* non-significant

limits collagen deposition [13]; *TIMP1* inhibits the degradation of the main components of the extracellular matrix [14]; and *SERPINE1* inhibits the dissolution of fibrinolysis [15]. The reduction of *CTHRC1* and elevation of *TIMP1* and *SERPINE1* expression helps explain the observed collagen accumulation in *LEPTIN*$^{-/-}$ livers.

Following additional H&E staining, PAS staining, Sirius red staining, Brunt's scoring criteria and Scheuer scoring criteria [16], the stage of non-alcoholic liver inflammation and fibrosis in *LEPTIN*$^{-/-}$ pigs was determined. The statistical results showed that the average NASH score was 4.47 ± 0.86 at 12–22 months in *LEPTIN*$^{-/-}$ pig. By 22–35 months, the average fibrosis score in *LEPTIN*$^{-/-}$ pig was 3.00 ± 0.27. In humans, the highest score observed clinically is 4.0. Thus, the stage of fibrosis in *LEPTIN*$^{-/-}$ pigs was clinically assessed in the range of moderate and severe (Table 2).

Porcine LEPTIN deficiency reduces JAK2-STAT3 signaling and enhances lipid peroxidation

To identify the mechanism driving liver fibrosis in *LEPTIN*$^{-/-}$ pigs, several signaling pathways proven to be affected by LEPTIN were analyzed. Utilizing WB and real-time PCR analyses, no significant changes in the expression of mTOR, MAPK and PI3K-AKT pathway related proteins and genes were observed (Fig. 4, Additional file 1: Fig. S6). Interestingly, phosphorylation of JAK2 and STAT3 was significantly reduced in *LEPTIN*$^{-/-}$ livers. In addition, altered expression of genes and proteins related to the JAK-STAT signaling pathway was also observed in response to LEPTIN deletion (Fig. 4A). The WB assay demonstrated that the phosphorylation of JAK2 and STAT3 was significantly reduced in *LEPTIN*$^{-/-}$ cells (Fig. 4A). In particular, SOCS3, a negative regulator of cytokines and hormone transduction [17], and SREBP-1c, related to fat synthesis [18] were analyzed. STAT directly inhibits SREBP-1c, and SOCS3 promotes SREBP-1c expression [19]. Both SOCS3 and SREBP-1c expression was elevated in *LEPTIN*$^{-/-}$ livers (Fig. 4B). Up-regulation of ACSL3 and ACSL5 in *LEPTIN*$^{-/-}$ indicates increased synthesis of acyl-CoA. The expression of CPT1a and CPT2 were also up-regulated in *LEPTIN*$^{-/-}$ livers, suggesting that FFA oxidation was activated. Immunofluorescence staining of SOCS3, SREBP1c and ACSL3 demonstrated increased expression in *LEPTIN*$^{-/-}$ fibrotic livers, suggesting that FFA synthesis was enhanced (Additional file 1: Fig. S7). In addition, the increased CPT1a and CPT2 expression suggested that acyl-coA transportation from the endoplasmic reticulum to mitochondria was enhanced (Fig. 4).

Since LEPTIN deficiency affects β-oxidation, genes involved in the oxidation process were analyzed: *ACAT1* and *ACAT2* are acyl-coA transferases; *ACADM, ACADS* and *ACADL* are acyl-coA dehydrogenases; *ACSL1, ACSL3* and *ACSL5* are acyl-coA synthetizes; *ACOT7, ACOT8* and *ACOT12* are acyl-coA thioesterases; *Cpt1a, Cpt1b, Cpt1c* and *Cpt2* are carnitine transferases. Among them, *ACAT2*, *ACSL1*, *ACSL3*, *ACSL5*, *ACOT7*, *CPT1A*, *CPT1B* and *CPT2* were significantly up-regulated. This suggested that β-oxidation has mainly been strengthened during acyl-coA synthesis and transfer to the mitochondria (Fig. 4C).

LEPTIN deficiency activates AMPK pathway and enhances gluconeogenesis and mitochondrial autophagy in pigs

Gluconeogenesis disorder is the most typical feature of insulin resistance in which HNF-4α synergizes with PGC-1α, FOXO1 and other key enzymes to induce gluconeogenesis [20], and Leptin regulates the AMPK pathway by inhibiting HNF-4α and promoting SIRT1 expression (21). In addition, PEPCK and G6Pase are speed limiting enzymes of glycogenesis [22]. Based on the conclusions of these previous studies, protein or gene expression levels of these markers in biological pathways or biochemical processes in *LEPTIN*$^{-/-}$ pig livers were detected. It confirmed that the lack of Leptin down-regulated phosphorylation of AMPK due to increased Hnf-4α and decreased SIRT1 expression in *LEPTIN*$^{-/-}$ pig livers. PEPCK and G6Pase were also significantly up-regulated (Fig. 4D, E). In addition, the fluorescence staining results demonstrate increased PEPCK and G6Pase expression with highly expressed α-SMA in *LEPTIN*$^{-/-}$ fibrotic livers, especially in the portal and perivenous areas (Fig. 4, Additional file 1: Fig. S8).

SIRT1 regulates mitochondrial autophagy and proliferation through PINK1/Parkin and PGC-1α/TFAM, respectively [23]. Initially markers of mitochondrial autophagy, Beclin1, LC3-II and P62 [24] were examined. The expression levels of PINK1 and phosphorylation of PARKIN were largely increased (Fig. 4F), and the expression of Beclin1, LC3-II and P62 were also significantly increased in *LEPTIN*$^{-/-}$ livers (Fig. 4G). In contrast with the autophagy related genes, most of the mitochondrial synthesis related genes were not altered in *LEPTIN*$^{-/-}$. No expression changes for the mtDNA genes *ATP6, COX1* and *ND1* were observed via qPCR (Fig. 4,

Table 2 Assessment of liver fibrosis and NASH staging in pigs

Type of Pig	NASH score (12–22 months)	Fibrosis score (22–35 months)
LEPTIN$^{-/-}$ *-1*	5.43	3.33
LEPTIN$^{-/-}$ *-2*	4.66	3.00
LEPTIN$^{-/-}$ *-3*	3.33	2.67
Mean ± SD	4.47 ± 0.86	3.00 ± 0.27
WT-1	0	0.67
WT-2	0.33	0.33
WT-3	0.67	0
Mean ± SD	0.33 ± 0.27	0.33 ± 0.27

Brunt's and Scheuer scoring criteria were used to determine the stage of non-alcoholic liver inflammation and fibrosis in *LEPTIN*$^{-/-}$ and WT pigs

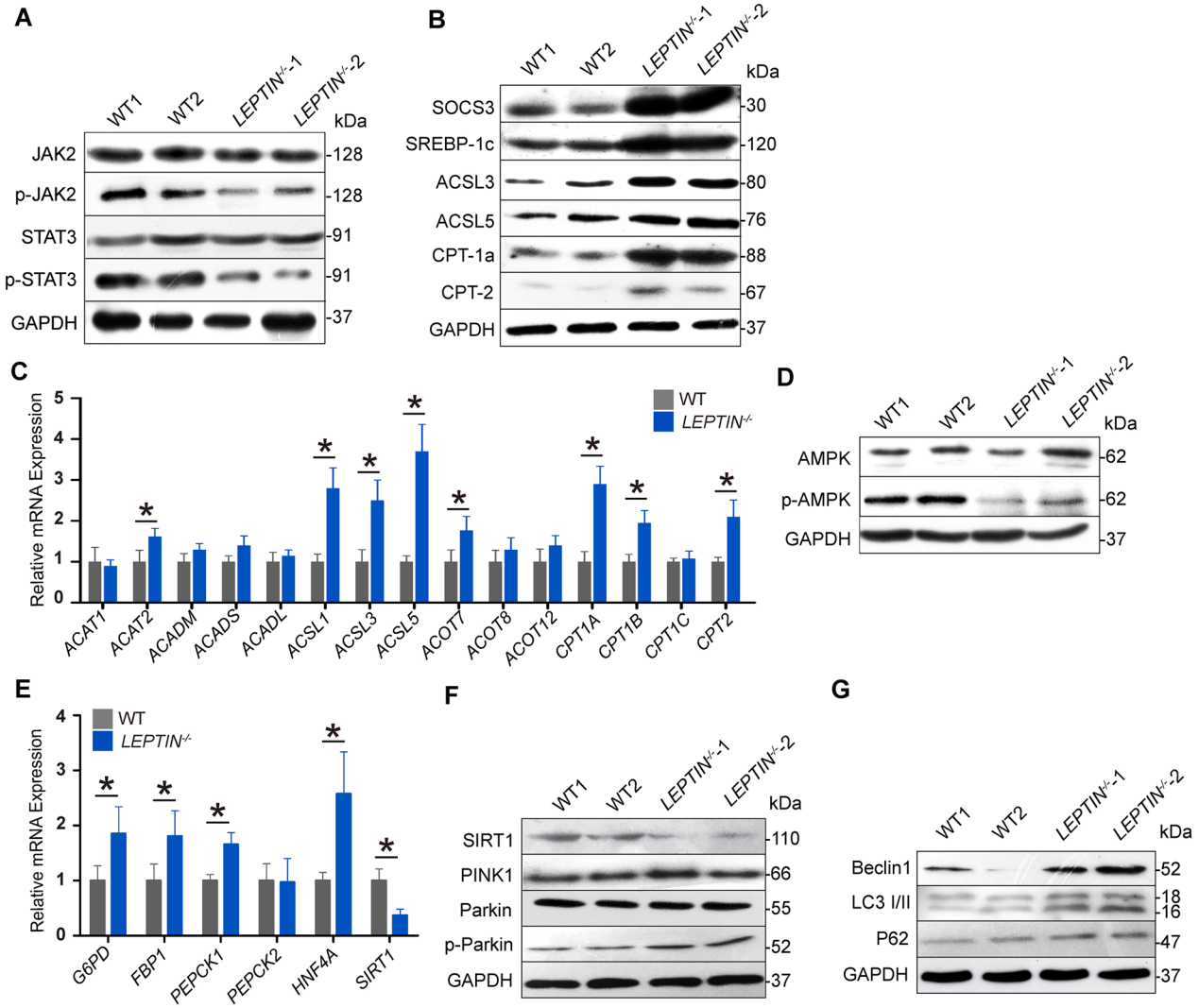

Fig. 4 Alteration of JAK-STAT and AMPK pathway related genes in *LEPTIN*$^{-/-}$ pig livers. **A** WB analysis of JAK-STAT signaling proteins. **B** WB analysis of FFA synthesis and oxidation related proteins. **C** Expression of β-oxidation related genes. **D** WB analysis of AMPK signaling proteins. **E** Expression of gluconeogenesis related genes. **F** WB analysis of SIRT1-mediated autophagy related proteins. **G** WB analysis of mitochondrial autophagy markers. N = 3/group. The bars represent the mean ± SD; *P < 0.05

Additional file 1: Fig. S9A). mtDNA copy number was calculated using Gcg as the internal reference, and the mtDNA copy number was not altered in *LEPTIN*$^{-/-}$ pig livers (Fig. 4, Additional file 1: Fig. S9B), suggesting that the down-regulation of SIRT1 in *LEPTIN*$^{-/-}$ pig livers enhances mitochondrial autophagy but does not affect mitochondrial synthesis.

LEPTIN$^{-/-}$ pigs undergo oxidative stress

Both lipid peroxidation and mitochondrial autophagy produce excessive ROS which in turn causes oxidative stress [25]. Heatmap analysis based on DEGs and expression difference fold change was performed using the Omicshare software (Fig. 5, Additional file 1: Fig. S10). GO enrichment analysis identified oxidation–reduction GO terms enriched for DEGs (Fig. 5, Additional file 1: Fig. S11). In addition, the CYP2 mediated arachidonic acid metabolism and exogenous toxic substances metabolic pathways were unexpectedly enriched for DEGs in *LEPTIN*$^{-/-}$ pig livers (Fig. 5, Additional file 1: Fig. S12, Table S2). Since the CYP2 enzyme mediates oxidative stress [26], real-time PCR was utilized to monitor the expression of CYP2 family genes (Fig. 5A). The level of CYP2E1 in *LEPTIN*$^{-/-}$ liver was nearly 3 times higher than in WT (Fig. 5B). The SOD enzyme activity was significantly reduced in *LEPTIN*$^{-/-}$ livers and sera, which

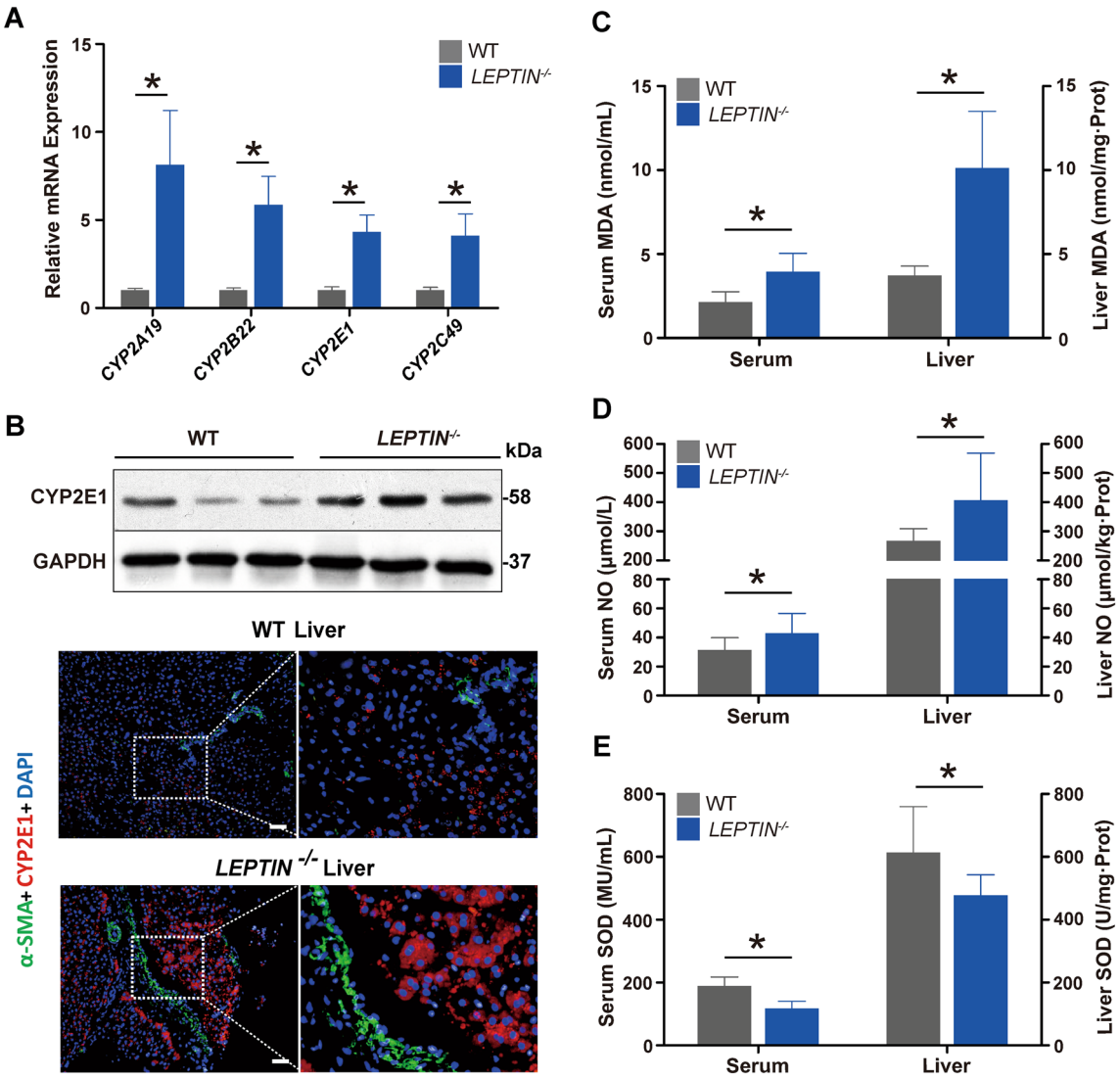

Fig. 5 Detection of oxidative stress in *LEPTIN*$^{-/-}$ pig livers. **A** Expression analysis of CYP2 family genes by real-time PCR. **B.** WB analysis and Immunofluorescence staining of CYP2E1. Scale bar represents 100 μm. **C**–**E** Detection of oxidative stress markers in the liver and serum. Content of MDA (**C**), NO (**D**) and SOD (**E**). N = 3/group. The bars represent the mean ± SD; *P < 0.05

could contribute to the excessive accumulation of ROS. Meanwhile, NO was up-regulated, and its reaction with OH increased the production of toxic ROS, which in turn led to increased MDA (Fig. 5C–E). These data indicate that LEPTIN deletion enhances oxidative stress in pig livers.

LEPTIN deficient rat livers are void of hepatic fibrosis, mitochondrial autophagy and oxidative stress

Interestingly, published studies and data presented in this study demonstrate that, in contrast with pigs, Leptin deficiency in rodents does not result in hepatic fibrosis [8, 9]. Compared with WT rats, the *Leptin*$^{-/-}$ rats at 12 months of age have larger body and liver sizes (Fig. 6A). H&E staining of *Leptin*$^{-/-}$ rat livers revealed fatty liver, lipid degeneration and balloon-like degeneration (Fig. 6B). Sirius red staining, α-SMA staining and the four serum hepatic fiber indicators analysis showed no obvious collagen accumulation and fibrogensis occurring in *Leptin*$^{-/-}$ rat livers (Fig. 6B, C). Furthermore, testing for SOD, MDA and NO found no obvious differences between *Leptin*$^{-/-}$ and WT rat livers (Fig. 6, Additional file 1: Fig. S 13A–C). This suggests that oxidative stress does not occur in *Leptin*$^{-/-}$ rat livers. WB and immunofluorescence staining revealed that the level of CYP2E1 was lowered (Fig. 6D, Additional file 1: Fig. S13D). To

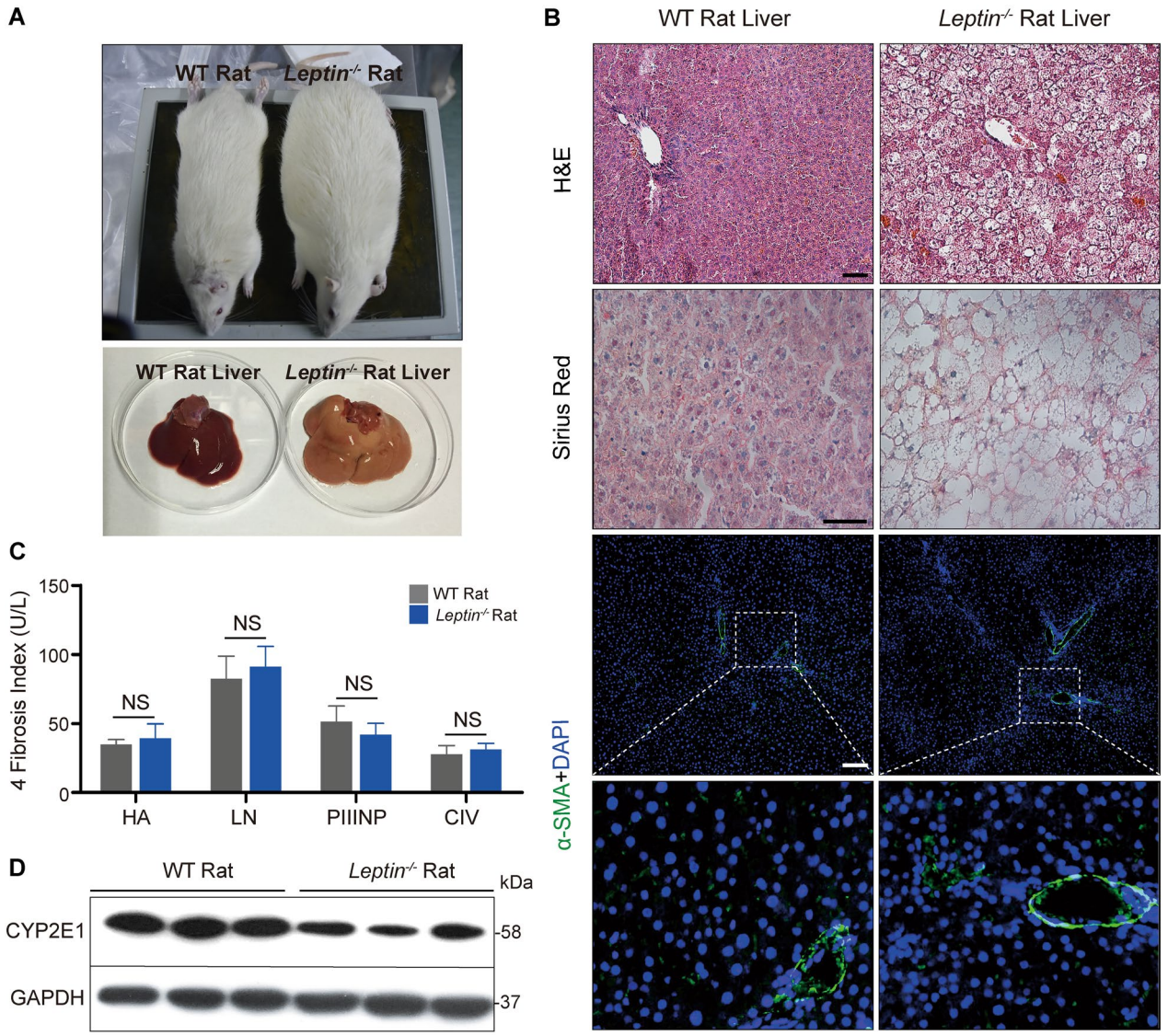

Fig. 6 Analysis of liver injury and related signaling pathways in *Leptin*$^{-/-}$ rats. **A** Comparison of *Leptin*$^{-/-}$ and WT rat bodies and livers. **B** H&E, Sirius red and α-SMA staining analysis of rat livers. Scale bar represents 100 μm. **C** Detection of fibrosis markers in serum.

investigate whether Leptin deletion in rats alters the JAK2-STAT3 pathway, p-JAK2/JAK2, p-STAT3/STAT3, SREBP-1C, SOCS3, CPT-1A and CPT-2 expressions were analyzed by WB and immuno-fluorescence staining. As observed in the *LEPTIN*$^{-/-}$ pig liver, the level of p-JAK2 and p-STAT3 were decreased compared to WT rat livers (Fig. 6, Additional file 1: Fig. S14A) whereas the SREBP-1C and SOCS3 were significantly increased in *Leptin*$^{-/-}$ rat livers (Fig. 6, Additional file 1: Fig. S14B, C), suggesting that the FFA synthesis was activated in *Leptin*$^{-/-}$ rat liver. However the expression of CPT-1A and CPT-2 in *Leptin*$^{-/-}$ rat livers were not altered (Fig. 6, Additional file 1: Fig. S14B, C).

Previous studies in pigs have demonstrated that Leptin deficiency promotes mitochondrial autophagy, representing another major source of oxidative stress. Therefore, mitochondrial autophagy related markers were examined. Beclin1, LC3-II and P62 expression showed no significant differences between *Leptin*$^{-/-}$ and control rats (Fig. 6, Additional file 1: Fig. S15A). It was interesting to note that, in contrast with *LEPTIN*$^{-/-}$ pigs, SIRT1 expression in *Leptin*$^{-/-}$ rat liver was up-regulated (Fig. 6, Additional file 1: Fig. S15B). This is quite different from

the results in pigs and may be a key reason why *Leptin*$^{-/-}$ rat livers do not have mitochondrial autophagy.

In order to investigate the underlying causes of this phenomenon of opposite trends in protein expression between the two animals, WB was performed to detect the phosphorylation of AMPK pathway related genes. Interestingly, in contrast with *LEPTIN*$^{-/-}$ pig, the phosphorylation of AMPK was significantly increased in *Leptin*$^{-/-}$ rats (Fig. 6, Additional file 1: Fig. S15C), providing a mechanism through which SIRT1 expression declined as SOCS3 and SREBP-1C expression increased.

Discussion

The liver closely communicates with adipose tissue and liver injury is observed in nearly 80% of obese patients [27]. Since mechanistic studies of liver fibrogenesis are difficult to conduct in patients, current knowledge of obesity-induced liver fibrosis is mainly derived from Leptin-deficient animal models. The choice of Leptin is based on its important roles in mediating energy homeostasis. Serum Leptin concentrations demonstrate an association with NAFLD which is mediated through insulin secretory dysfunction and insulin resistance in obese patients [28]. NAFLD, the hepatic manifestation of the metabolic syndrome, comprises steatosis, steatohepatitis, hepatic fibrosis, cirrhosis and hepatocellular carcinoma [29]. However, both previously published studies and work presented here suggests that two of the most commonly used rodent models, *ob/ob* mouse and Zucker rat, do not develop fibrosis observed in NAFLD patients. In an effort to develop a model that displays fibrogenesis as observed by patients, a *LEPTIN*$^{-/-}$ pig model was created. Consistent with human clinical data, the *LEPTIN*$^{-/-}$ pigs demonstrated obstructed body glucose regulation leading to insulin resistance and type II diabetes by 12-months of age. Interestingly, around the same age [6–12], 60% of *LEPTIN*$^{-/-}$ pig livers displayed lipid deposition and hepatocyte steatosis. The severity of liver injury also worsened with age in *LEPTIN*$^{-/-}$ pigs. Lobular inflammation and hepatocyte ballooning appeared in 33% *LEPTIN*$^{-/-}$ of pig livers between 12–22 months, whereas 42.9% *LEPTIN*$^{-/-}$ pig livers developed various degrees of fibrosis by 22–35 months of age (Fig. 2). The development of liver injury in *LEPTIN*$^{-/-}$ pigs mirrored the pathological progression of NAFLD observed in obese patients. *LEPTIN*$^{-/-}$ pigs appeared to closely model the process of fibrogenesis observed in patients, which supports their use for investigation of the mechanisms underlying fibrogenesis in patients.

The mechanisms leading to NAFLD are unclear to date. In obese subjects, FFAs seem to be misrouted to ectopic sites like hepatic tissues, resulting in steatosis. Steatosis induces the production of pro-inflammatory mediators like TNF-α, IL-6 and IL-1β. These cytokines promote the recruitment and activation of Kupffer cells, which induce inflammation and hepatic insulin resistance via SOCS3. The accumulation of fat in the liver leads to lipotoxicity and dysfunctional mitochondria, which further causes oxidative stress due to imbalanced ROS production and protective oxidants, eventually leading to hepatocyte death in NAFLD patients. The reduced phosphorylation of JAK2 and STAT3 in LEPTIN deficient pig livers led to hepatic insulin resistance and increased fat synthesis marked by activation of SOCS3 and SREBP-1c, respectively, further confirms the value of the pig model (Fig. 4). This data is consistent with observed alterations in the JAK/STAT pathways in the pathogenesis of metabolic disease [30]. The excess intracellular FFAs observed in *LEPTIN*$^{-/-}$ pigs resulted in intrinsic endoplasmic reticulum stress. The toxic pathways were represented through the generation of ROS and increased mitochondrial β-oxidation, which further caused hepatocyte death and fibrosis. Interestingly, in contrast with pigs, although the Leptin deletion in rats altered the JAK2 and STAT3 phosphorylation and caused fatty liver, the level of damage was not severe enough to drive mitochondrial β-oxidation and oxidative stress, which may explain why fibrosis did not occur in *Leptin*$^{-/-}$ rat livers (Fig. 6).

The progression of NAFLD to NASH has been characterized as a mitochondrial disease occurring at an early human disease stage [31]. Lipotoxicity encompasses the dysregulation of the intracellular lipid composition, resulting in mitochondria dysfunction, stimulating ROS production, oxidative stress, and impaired FFA oxidation [32, 33]. AMPK is a heterotrimeric enzyme which regulates cell growth, proliferation, autophagy and apoptosis [34]. In NAFLD, activation of AMPK in the liver inhibits the synthesis and oxidation of FFAs, leading to the reduction of ectopic lipid accumulation and improved insulin action [35]. The current study on *Leptin*$^{-/-}$ rats provided evidence that AMPK activation might be crucial for prevention of liver damage. This is further supported by the observed inactivation of the AMPK pathway in *LEPTIN*$^{-/-}$ pigs, which drove mitochondrial autophagy, hepatic cell death and fibrosis. Whether LEPTIN is required for activation of the AMPK pathway, or AMPK mediated autophagy appears as a defensive reaction to liver injury has not been previously addressed in the pig. The gene regulatory network architecture plays a key role in explaining the biological differences between species. A numerous factor regulates the activities of AMPK in pig and rat. The analyses in the present study suggest the likelihood that species differences in one or a combination of those factors may participate in AMPK regulation. Additionally, since components of dietary fiber may influence gene expression indirectly through

changes in hormonal signaling and metabolites produced by the intestinal microflora, whether the distinct nutritional content contributes to the difference in phenotype remains to be determined. Identification of genes in liver cells that are differentially regulated by dietary fiber will be an important step toward understanding the role of dietary factors in fibrosis progression. Nevertheless, one collective conclusion from our study is that the activity of AMPK represents a potential predictive biomarker of the severity of liver injury. Activation of AMPK using pharmacological agents may also represent a potential therapeutic avenue for preventing the progress of NASH to fibrosis.

Liver fibrosis is defined by the excessive accumulation of extracellular matrix (ECM) proteins. Activated hepatic stellate cells (HSCs) in the liver are the major source of collagen production, leading to an imbalance in the formation and degradation of the ECM. Activation of HSCs in the injured liver is regulated by fibrogenic and pro-inflammatory cytokines [36]. Recent evidence demonstrated that adiponectin induces apoptosis and inhibits its activation of HSCs through the AMPK pathway [37]. Thus, the reduced AMPK signaling observed in *LEPTIN*$^{-/-}$ pig livers may promote the activation of HSCs, which in turn induce the deposition of ECM proteins and development of fibrosis; whereas the activated AMPK in *Leptin*$^{-/-}$ rat livers may lead to the apoptosis of HSCs, preventing the accumulation of ECM proteins.

The underlying mechanisms by which NASH transitions to fibrosis are not completely understood. Hepatic fibrosis occurs in 40–50% of patients with NASH and approximately 30–40% of NAFLD patients develop NASH. It has been estimated that the hepatic fibrosis stage is the strongest predictor of mortality in NAFLD patients. The present understanding of the dynamics in NAFLD progression has emerged from genetically modified rodents, such as *ob/ob* mice and Zucker rats. These animals are universally used in obesity and diabetic research. However, they fail to develop hepatic fibrosis.

Conclusions

The LEPTIN deficient pigs generated in this study mirror the progression of hepatic fibrosis observed in NAFLD patients. Loss of LEPTIN in pigs led to β-oxidation and oxidative stress and, in combination with AMPK mediated mitochondrial autophagy, increased liver fibrosis (Fig. 7). In sum, LEPTIN-deficient pigs provide an ideal model to investigate the full spectrum of human NAFLD

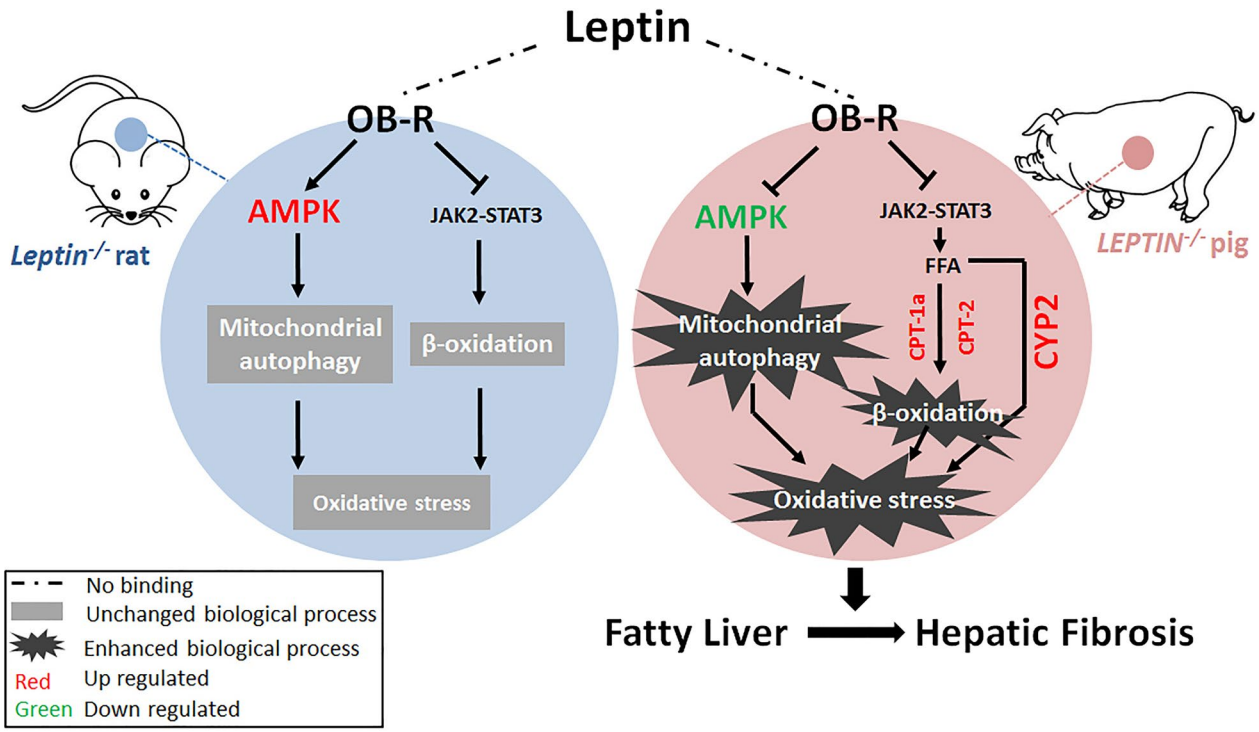

Fig. 7 Proposed mechanistic model of fibrosis progression in *LEPTIN*$^{-/-}$ pig liver. Reduction of p-AMPK promotes mitochondrial autophagy. Meanwhile, activation of JAK2/STAT3 signaling pathway leads to enhanced FFA oxidation and oxidative stress. Oxidative stress drives the development liver fibrosis in *LEPTIN*$^{-/-}$ pigs

and develop new strategies for the diagnosis and treatment of NAFLD.

Methods

Animal experiments were approved by the Animal Care Committee of the China Agricultural University (Plan book number SKLAB-2016–84) and performed according to the Chinese Animal Welfare Act. All chemicals used were purchased from Sigma-Aldrich Co. (Alcobendas, Madrid, Spain) unless otherwise indicated.

Experimental animals

The pig species used to generate *LEPTIN*$^{-/-}$ pigs was the Chinese experimental mini-pig [10]. Both wild type and *LEPTIN*$^{-/-}$ pigs were provided with same manufactured diet. The cereal grain in dry form has been ground to supply to the pigs using an ad libitum feeding at fixed time (7:00–8:00, 1.75 kg max; 12:00–13:00, 1.25 kg max; and 17:00–18:00, 1 kg max) every day. Formula feed is premixed based on the animal's nutritional requirements to meet different stages of growth. The nutrition content per kg premix formula feed is listed in Table 1. The *Leptin*$^{-/-}$ *r*ats were generated by the Sen Wu laboratory [11]. Both wild type and *Leptin*$^{-/-}$ rats were provided with the same always abundant manufactured diet (Table 1).

Generation of *LEPTIN*$^{-/-}$ pigs

Zinc finger nuclease (ZFN) plasmids targeting the *LEPTIN* gene were designed by Sigma-Aldrich. Fetal fibroblasts were isolated from 30-day old male pig embryo. Approximately 1×10^6 CEMP fetal fibroblasts were transfected with 2 μg of each ZFN vector. Following G418 selection (500 μg/mL, Promega), positive clones were collected for somatic cell nuclear transfer. PCR was performed following by Sanger sequencing to confirm the genetic sequence of the *LEPTIN* target region (primer sequence: Forward 5'-GATTGTGTGGAAGGGGAA GA-3', Reverse 5'-GAGGTCCGCACAGGCTCTC T-3'.

Western blotting (WB)

Total protein of adipose tissue, liver tissue, hypothalamus tissue and serum were obtained from the mutant and wild-type pigs. Electrophoretically separated proteins were detected by specific primary antibodies (Additional file 1: Table S3).

Enzyme linked immunosorbent assay (ELISA)

Serum was isolated from blood collected from pigs after fasting overnight. ELISA kit was used to detect porcine IL-1β, IL-6 and TNF-α (Dan Shi Biological Technology, Shanghai).

Growth parameters and body composition

Body weight of *LEPTIN*$^{-/-}$ and control pigs were examined weekly or monthly. The percentage of total body fat was determined by using multi-slice computed tomography (MSCT) with 64 rows, 128-slice MSCT scanner (Siemens). MSCT was performed with the following parameters: 120 kV, 500 ms, and 1.5 mm splice thickness. The 3D reconstruction and analysis of data were performed by Sygo Fastview software.

Assessment of clinical indicators of liver disease

Triglycerides, insulin, cholesterol, HDL, LDL, AST, ALT, ALP and four indexes of hepatic fibrosis were analyzed by the Beijing CIC Clinical Laboratory, China Agricultural University Veterinary Teaching Hospital and the endocrinology department of Beijing Tongren Hospital.

HOMA model assessing type II diabetes

Homeostatic model assessment (HOMA) included the following values, calculated on the basis of two parameters of fasting plasma glucose and insulin: HOMA-IR = (FPG, mmol/L) × (FINS, mIU/L)/22.5, assessment of insulin resistance; HOMA-IS = 1/(FPG, mmol/L) × (FINS, mIU/L), assessment of insulin sensitivity; HOMA-β = 20 × (FPG, mmol/L)/[(FPG, mmol/L)-3.5] (%), assessment of islet β cell function. FPG, Fasting plasma glucose and FINS, fasting insulin.

Intravenous glucose tolerance test (IVGTT)

After 12-15 hours of fasting, pig blood samples were collected from the anterior chamber vein. 50% glucose solution was injected into the ear vein with a dose of 1.2mL/kg. Glucose concentrations were measured at 0 min (before injection), 1 min, 5 min, 10 min, 15 min, 30 min, 60 min and 90 min (after injection).

Histological analysis

Adipose, liver and pancreatic tissues were fixed in 10% neutral buffered formalin solution and paraffin-embedded. 5 μm-thick sections were used for hematoxylin–eosin (H&E) analysis, oil red O dye detection, periodic acid schiff (PAS) analysis (Beijing Solarbio life science), and Sirius red (Beijing Solarbio life science) analysis. α-SMA (ab5694, abcam) antibody was used for immunofluorescence using the ABC method (Vector Laboratories).

RNA isolation and quantitative RT-PCR

Total RNA was isolated from pig fat or liver tissues by TRIzol and RNeasy Mini Kit (QIAGEN). Then RNA samples were reverse transcribed to cDNA by M-MLV reverse transcription kit (Promega). The levels of relevant mRNAs were quantitated by real-time PCR using

One Step SYBR GREEN RT-PCR Kit (Roche) in a Light Cycler instrument (Roche Applied Science, Mannheim, Germany). The specific primers for related genes were designed by Primer3 (v.0.4.0), PrimerBank, primer premier5.0 and NCBI BLAST (Additional file 1: Table S4).

Detection of oxidative stress markers

Blood samples were collected from pigs after fasting overnight. Liver tissue was homogenized in cold 0.9% normal saline. The determination of NO requires the use of a specific homogenate. The total SOD activity detection kit (WST-8 method) (Beyotime, S-0101), lipid oxidation (MDA) assay kit (Beyotime, S-0131) and nitric oxide detection kit (Beyotime, S-0021) were utilized following the manufacturer's instructions.

Transcriptome analysis

The total liver RNA of three *LEPTIN*$^{-/-}$ and WT pigs from 22–35 month of age was extracted. The library construction and sequencing were performed with the steps of purifying mRNA, interrupting mRNA, synthesizing cDNA, selecting fragments, and PCR amplification. The qualified libraries were generated on Illumina Cbot for cluster generation, and then Illumina HiSeqTM2500 was used for transcriptome Sequencing. The purity, concentration and integrity of RNA samples were measured by Nano Drop, Qubit 2.0 and Agilent 2100 before sequencing. The cDNA library was constructed using the Illumina TruseqTM RNA kit (Illumina, USA). The sequencing read length is PE125. Nearly 50 GB per sample of raw data was obtained by sequencing, and 6-8 GB clean data of each sample was obtained after removal of reads containing low sequencing quality with connectors and duplicates. After clean reads were obtained, HISAT was used for sequence alignment with the reference genome (Sus_scrofa. Sscrofa10.2.dna.chromosome) to obtain the information of the reference genes and the Mapped reads were obtained. By using the Cuffdiff component of Cufflinks software, the gene expression levels were quantified. Pearson's correlation co-efficient (r^2) was used as an indicator to evaluate the biological correlation of repetition. Then FPKM was used to determine the expression abundance of transcripts. The absolute value of Log2 Fold Change ≥ 1, and the corrected P value (FDR) < 0.05, was taken as the key index to screen the differential genes. GO and KEGG software were used for differential genes enrichment and signaling pathways screening. In GO and KEGG analysis, $P < 0.05$ was used as the selection criteria. DAVID and KOBAS software were used for gene function analysis. The RNA-Seq data was deposited in Gene Expression Omnibus (GEO) under the accession number GSE176023.

Statistical analysis

The experimental data are presented as the mean ± SD and were analysed by paired Student's *t* test using SPSS15.0 software to compare the mutant and wild-type pigs. *P* value < 0.05 was considered significant.

Abbreviations

ACADL	Acyl-CoA dehydrogenase long chain
ACADM	Acyl-CoA dehydrogenase medium chain
ACADS	Acyl-CoA dehydrogenase short chain
ACAT1/2	Acetyl-CoA acetyltransferase 1/2
ACOT7/8/12	Acyl-CoA thioesterase 7/8/12
ACSL1/3/5	Acyl-CoA synthetases 1/3/5
ACTA2	Alpha-actin 2
ALP	Alkaline phosphatase
ALT	Alanine aminotransferase
AMPK	AMP-activated protein kinase
AST	Aspartate aminotransferase
ATP6	Mitochondrial ATPase subunit 6
CEMP	Chinese miniature experiment pig
CIC	China isotope corporation
CIV	Collagen type IV
COL1A1	Collagen Type I Alpha 1
COX1	Mitochondrial Cytochrome c oxidase subunit I
CPT 1A/1B/2	Carnitine palmitoyltransferase 1A/1B/2
CTHRC1	Collagen triple helix repeat containing 1
DEGs	Differentially expressed genes
ECM	Extracellular matrix
ELISA	Enzyme linked immunosorbent assay
ELOVL6	Elongaseofverylongchainfattyacids 6
FABP1	Fatty acid binding protein
FASN	Fatty acid synthetase
FDR	False discovery rate
FFA	Free fatty acid
FINS	Fasting plasma insulin
FPG	Fasting plasma glucose
G6Pase	Glucose-6 phosphatase
GAPDH	Glyceraldehyde-3-phosphate dehydrogenase
GO	Gene ontology
H&E	Hematoxylin–eosin
HA	Hyaluronic acid
HDL	High density lipoprotein
HISAT	Hierarchical indexing for spliced alignment of transcripts
HNF-4α	Hepatocyte nuclear factor 4-alpha
HOMAs	Homeostasis model assessment
HSCs	Hepatic stellate cells
IL-1β/6	Interleukin 1 beta/6
IR	Insulin resistance
IS	Insulin sensitivity
IVGTT	Intravenous glucose tolerance test
JAK2	Janus kinase 2
KEGG	Kyoto encyclopedia of genes and genomes
LC3	Microtubule associated protein 1 light chain 3
LDL	Low density lipoprotein
LN	Laminin
LRAT	Lecithin retinol acyltransferase
MCP-1	Monocyte chemotactic protein 1
MDA	Malondialdehyde

MSCT	Multi-slice computed tomography
NAFLD	Non-alcoholic fatty liver disease
NASH	Non-alcoholic steatohepatitis
ND1	Mitochondrial NADH-ubiquinone oxidoreductase chain 1
NFKB	Nuclear factor kappa-light-chain-enhancer of activated B cells
NO	Nitric oxide
PAS	Periodic acid schiff
PEPCK	Phosphoenolpyruvate carboxylase
PGC-1α	Peroxisome proliferator activated receptor gamma coactivator 1 alpha
PIIINP	Procollagen-III-peptide
PINK1	Phosphatase and tensin homolog induced kinase 1
PPARA	Peroxisome proliferator-activated receptor alpha
ROS	Reactive oxygen species
SCD1	Stearoyl-CoA desaturase 1
SERPINE1	Serpin family E member 1
SIRT1	Sirtuin 1
SOCS-3	Suppressor of cytokine signaling-3
SOD	Superoxide dismutase
SREBP-1c	Sterol-regulatory element-binding protein-1c
STAT3	Signal transducer and activator of transcription 3
TFAM	Transcription factor A, mitochondrial
TGFB	Transforming growth factor-beta
TIMP1	Tissue inhibitor of matrix metalloprotease-1
TNF-α	Tumor necrosis factor alpha
WB	Western blotting
WT	Wild type
ZFN	Zinc finger nuclease technology
α-SMA	Alpha smooth muscle actin

Supplementary Information

The online version contains supplementary material available at https://doi.org/10.1186/s13578-023-01124-1.

Additional file 1. Additional figures and tables.

Acknowledgements
We are grateful for the gift of *Leptin*$^{-/-}$ pigs by Dr. Ning Li and *Leptin*$^{-/-}$ rats by Dr. Sen Wu. We would like to acknowledge the helps of Dr. Changgong Li for technical supporting and Dr. Lennart Hammarstrom for manuscript writing.

Author contributions
TT, ZS, WL, RW, MZ and YB performed the experiments; ZL, QW, HW and XH analyzed the data; YX conceived and designed the experiments, and wrote the manuscript with input from all authors. All authors have read and approved the manuscript.

Funding
This work was supported by the National Natural Science Foundation of China (31972566) and Plan 111 (B12008). The funding body played no role in the design of the study and collection, analysis, and interpretation of data and in writing the manuscript.

Availability of data and materials
All data generated or analyzed during this study are included in this published article and its supplementary information files.

Declarations

Ethics approval and consent to participate
This study was approved by the Animal Care Committee of the China Agricultural University (Plan book number SKLAB-2016–84) and performed according to the Chinese Animal Welfare Act.

Consent for publication
Not applicable.

Competing interests
The authors declare that they have no competing of interest.

Received: 5 July 2023 Accepted: 31 August 2023
Published online: 13 September 2023

References

1. Brunt EM. Nonalcoholic steatohepatitis. Semin Liver Dis. 2004;24(1):3–20.
2. Hebbard L, George J. Animal models of nonalcoholic fatty liver disease. Nat Rev Gastroenterol Hepatol. 2011;8(1):35–44.
3. Asrani SK. Liver transplantation for nonalcoholic steatohepatitis. Clin Gastroenterol Hepatol. 2014;12(3):403–4.
4. Browning JD, Horton JD. Molecular mediators of hepatic steatosis and liver injury. J Clin Invest. 2004;114(2):147–52.
5. Weisberg SP, McCann D, Desai M, Rosenbaum M, Leibel RL, Ferrante AW. Obesity is associated with macrophage accumulation in adipose tissue. J Clin Invest. 2003;112(12):1796–808.
6. Romboms K, Marraf F. Molecular mechanisms of hepatic fibrosis in Non-alcoholic steatohepatitis. Dig Dis. 2010;28(1):229–1235.
7. Farooqi IS, O'Rahilly S. Leptin: a pivotal regulator of human energy homeostasis. Am J Clin Nutr. 2009;89(3):980S-984S.
8. Leclercq IA, Farrell GC, Schriemer R, Robertson GR. Leptin is essential for the hepatic fibrogenic response to chronic liver injury. J Hepatol. 2002;37(2):206–13.
9. Ikejima K, Takei Y, Honda H, Hirose M, Yoshikawa M, Zhang YJ, et al. Leptin receptor-mediated signaling regulates hepatic fibrogenesis and remodeling of extracellular matrix in the rat. Gastroenterology. 2002;122(5):1399–410.
10. Fan B, Yang SL, Liu B, Yu M, Zhao SH, Li K. Characterization of the genetic diversity on natural populations of Chinese miniature pig breeds. Anim Genet. 2003;34(6):465–6.
11. Lan H, Li S, Guo Z, Men H, Wu Y, Li N, et al. Efficient generation of selection-gene-free rat knockout models by homologous recombination in ES cells. FEBS Lett. 2016;590(19):3416–24.
12. Machado M, Marques-Vidal P, Cortez-Pinto H. Hepatic histology in obese patients undergoing bariatric surgery. J Hepatol. 2006;45(4):600–6.
13. LeClair R, Lindner V. The role of collagen triple helix repeat containing 1 in injured arteries, collagen expression, and transforming growth factor beta signaling. Trends Cardiovasc Med. 2007;17:202–5.
14. Giannandrea M, Parks WC. Diverse functions of matrix metalloproteinases during fibrosis. Dis Model Mech. 2014;7(2):193–203.
15. Ghosh AK, Vaughan DE. PAI-1 in tissue fibrosis. J Cell Physiol. 2012;227:493–507.
16. Farrell GC, Chitturi S, Lau GK, Sollano JD. Asia-Pacific Working Party on NAFLD. Guidelines for the assessment and management of non-alcoholic fatty liver disease in the Asia-Pacific region: executive summary. J Gastroenterol Hepatol 2007; 22(6): 775–777.
17. Yumet G, Shumate ML, Bryant DP, Lang CH, Cooney RN. Hepatic growth hormone resistance during sepsis is associated with increased suppressors of cytokine signaling expression and impaired growth hormone signaling. Crit Care Med. 2006;34(5):1420–7.
18. Joseph SB, Laffitte BA, Patel PH, Watson MA, Matsukuma KE, Walczak R, et al. Direct and indirect mechanisms for regulation of fatty acid synthase gene expression by liver X receptors. J Biol Chem. 2002;277(13):11019–25.
19. Ueki K, Kondo T, Tseng YH, Kahn CR. Central role of suppressors of cytokine signaling proteins in hepatic steatosis, insulin resistance, and the metabolic syndrome in the mouse. P Natl Acad Sci USA. 2005;102(38):10422–7.
20. Mcglacken-Byrne SM, Hawkes CP, Flanagan SE, Ellard S, McDonnell CM, Murphy NP. The evolving course of HNF4A hyperinsulinaemic hypoglycaemia-a case series. Diabetic Med. 2014;31(1):E1–5.
21. Yu JW, Sun LJ, Liu W, Zhao YH, Kang P, Yan BZ. Hepatitis C virus core protein induces hepatic metabolism disorders through down-regulation of the SIRT1-AMPK signaling pathway. Int J Infect Dis. 2013;17:e539-545.

22. Goto M, Yoshioka T, Battelino T, Ravindranath T, Zeller WP. TNF alpha decreases gluconeogenesis in hepatocytes isolated from 10-day-old rats. Pediatr Res. 2001;49(4):552–7.
23. Sha D, Chin LS, Li L. Phosphorylation of parkin by Parkinson disease-linked kinase PINK1 activates parkin E3 ligase function and NF-kappaB signaling. Hum Mol Genet. 2010;19(2):352–63.
24. Scarlatti F, Maffei R, Beau I, Codogno P, Ghidoni R. Role of non-canonical Beclin 1-independent autophagy in cell death induced by resveratrol in human breast cancer cells. Cell Death Differ. 2008;15(8):1318–29.
25. Lee J, Ellis JM, Wolfgang MJ. Adipose fatty acid oxidation is required for thermogenesis and potentiates oxidative stress-induced inflammation. Cell Rep. 2015;10(2):266–79.
26. Leung TM, Nieto N. CYP2E1 and oxidant stress in alcoholic and non-alcoholic fatty liver disease. J Hepatol. 2013;58:395–8.
27. Williams CD, Stengel J, Asike MI, Torres DM, Shaw J, Contreras M, et al. Prevalence of Nonalcoholic Fatty Liver Disease and Nonalcoholic Steatohepatitis Among a Largely Middle-Aged Population Utilizing Ultrasound and Liver Biopsy: A Prospective Study. Gastroenterology. 2011;140(1):124–31.
28. Hossain IA, Akter S, Rahman MK, Ali L. Gender specific Association of Serum Leptin and Insulinemic Indices with nonalcoholic fatty liver disease in Prediabetic subjects. PLoS ONE. 2015;10(11): e0142165.
29. Odenthal MT, Sminia ML, Prick LJ, Gortzak-Moorstein N, Völker-Dieben HJ. Long-term follow-up of the corneal endothelium after artisan lens implantation for unilateral traumatic and unilateral congenital cataract in children - Two case series. Cornea. 2006;25(10):1173–7.
30. Penas-Steinhardt A, Tellechea ML, Gomez-Rosso L, Brites F, Frechtel GD, Poskus E. Association of common variants in JAK2 gene with reduced risk of metabolic syndrome and related disorders. BMC Med Genet. 2011;12:166.
31. Pessayre D, Fromenty B. NASH: a mitochondrial disease. J Hepatol. 2005;42(6):928–40.
32. Vial G, Dubouchaud H, Couturier K, Cottet-Rousselle C, Taleux N, Athias A. Effects of a high-fat diet on energy metabolism and ROS production in rat liver. J Hepatol. 2011;54:348–56.
33. Jeon SM. Regulation and function of AMPK in physiology and diseases. Exp Mol Med. 2016;48(7): e245.
34. Smith BK, Marcinko K, Desjardins EM, Lally JS, Ford RJ, Steinberg GR. Treatment of Nonalcoholic Fatty Liver Disease: Role of AMPK. Am J Physiol Endocrinol Metabol. 2016;311:E730–40.
35. Bataller R, Brenner DA. Liver fibrosis. J Clin Invest. 2005;115:209–18.
36. Luedde T, Schwabe RF. NF-κB in the liver–linking injury, fibrosis and hepatocellular carcinoma. Nat Rev Gastroenterol Hepatol. 2011;8:108–18.
37. Byrne CD, Targher G. NAFLD: a multisystem disease. Hepatol. 2015;62(1):S47–64.

Publisher's Note